Supplemental material to this article can be found at:
http://molpharm.aspetjournals.org/content/suppl/2021/07/02/molpharm.121.000303.DC1
1521-0111/100/3/283–294$35.00
MOLECULAR PHARMACOLOGY
https://doi.org/10.1124/molpharm.121.000303
Mol Pharmacol 100:283–294, September 2021

The Benzene Hematotoxic and Reactive Metabolite 1,4-Benzoquinone Impairs the Activity of the Histone Methyltransferase SET Domain Containing 2 (SETD2) and Causes Aberrant Histone H3 Lysine 36 Trimethylation (H3K36me3)[S]

Jérémy Berthelet[1], Christina Michail, Linh-Chi Bui, Louise Le Coadou, Valentina Sirri, Li Wang, Nicolas Dulphy, Jean-Marie Dupret, Christine Chomienne, Fabien Guidez, and Fernando Rodrigues-Lima

Université de Paris, Unité de Biologie Fonctionnelle et Adaptative (BFA), UMR 8251, CNRS, Paris, France (J.B., C.M., L.-C.B., L.L.C., V.S., J.-M.D., F.R.-L.); The First Affiliated Hospital of Chongqing Medical University, Department of Hematology, Chongqing, China (L.W.); Université de Paris, Institut de Recherche Saint-Louis (IRSL), UMRS 1160 (N.D.), UMRS 1131 (C.C., F.G.), INSERM, Paris, France; and Service de Biologie Cellulaire, Assistance Publique des Hôpitaux de Paris (AP-HP), Hôpital Saint Louis, Paris, France (C.C.)

Received April 15, 2021; accepted June 28, 2021

ABSTRACT

Human SETD2 is the unique histone methyltransferase that generates H3K36 trimethylation (H3K36me3), an epigenetic mark that plays a key role in normal hematopoiesis. Interestingly, recurrent inactivating mutations of SETD2 and aberrant H3K36me3 are increasingly reported to be involved in hematopoietic malignancies. Benzene (BZ) is a ubiquitous environmental pollutant and carcinogen that causes leukemia. The leukemogenic properties of BZ depend on its biotransformation in the bone marrow into oxidative metabolites, in particular 1,4-benzoquinone (BQ). This hematotoxic metabolite can form DNA and protein adducts that result in the damage and the alteration of cellular processes. Recent studies suggest that BZ-dependent leukemogenesis could depend on epigenetic perturbations, notably aberrant histone methylation. We investigated whether H3K36 trimethylation by SETD2 could be impacted by BZ and its hematotoxic metabolites. Herein, we show that BQ, the major leukemogenic metabolite of BZ, inhibits irreversibly the human histone methyltransferase SETD2, resulting in decreased H3K36me3. Our mechanistic studies further indicate that the BQ-dependent inactivation of SETD2 is due to covalent binding of BQ to reactive Zn-finger cysteines within the catalytic domain of the enzyme. The formation of these quinoprotein adducts results in loss of enzyme activity and protein crosslinks/oligomers. Experiments conducted in hematopoietic cells confirm that exposure to BQ results in the formation of SETD2 crosslinks/oligomers and concomitant loss of H3K36me3 in cells. Taken together, our data indicate that BQ, a major hematotoxic metabolite of BZ, could contribute to BZ-dependent leukemogenesis by perturbing the functions of SETD2, a histone lysine methyltransferase of hematopoietic relevance.

SIGNIFICANCE STATEMENT

Benzoquinone is a major leukemogenic metabolite of benzene. Dysregulation of histone methyltransferase is involved in hematopoietic malignancies. This study found that benzoquinone irreversibly impairs SET domain containing 2, a histone H3K36 methyltransferase that plays a key role in hematopoiesis. Benzoquinone forms covalent adducts on Zn-finger cysteines within the catalytic site, leading to loss of activity, protein crosslinks/oligomers, and concomitant decrease of H3K36me3 histone mark. These data provide evidence that a leukemogenic metabolite of benzene can impair a key epigenetic enzyme.

Introduction

Benzene (BZ) is an aromatic compound of industrial importance that is predominantly used as a solvent or as a primary material for chemical synthesis. BZ is also a carcinogen considered to be a ubiquitous environmental pollutant (Smith, 2010). Exposure to BZ is indeed a well established cause of hematopoietic malignancies (Smith et al., 2011; McHale et al., 2012; Snyder, 2012; Eastmond et al., 2014). The leukemogenic properties of BZ are known to rely on its metabolization in bone marrow cells into oxidative species, notably 1,4-benzoquinone (BQ) (Smith, 2010). This oxidative phenolic species is thought to be one of the major hematotoxic metabolites of BZ (Frantz et al., 1996; Whysner et al., 2004; Smith, 2010; Holmes and

This work was supported by running grants from Université de Paris and Centre National de la Recherche Scientifique, and by grants from ANSES (Agence Nationale de Sécurité Sanitaire de l'Alimentation, de l'Environnement et du Travail) and Instituts Thématiques MultiOrganismes Cancer (plan Cancer-Environnement). J.B. was supported by a Ph.D. fellowship from Cancéropole IDF (Région Ile de France), C.M. and L.L.C. are supported by Ph.D. fellowships from Université de Paris (Ecole Doctorale BioSPC).
The authors declare no conflict of interest.
[1]Current affiliation: Université de Paris, Centre Epigénétique et Destin Cellulaire (CEDC), UMR 7216, CNRS, Paris, France.
https://dx.doi.org/10.1124/molpharm.121.000303.
[S] This article has supplemental material available at molpharm.aspetjournals.org.

Winn, 2019; North et al., 2020). BQ is known to be particularly reactive and capable of binding proteins through Michael addition on certain reactive cysteine residues (Wang et al., 2006; Bolton and Dunlap, 2017). Although the mechanisms by which BZ induces hematologic malignancies remain poorly understood, different studies indicate that BZ metabolites act through multiple modes of action (McHale et al., 2012; Sauer et al., 2018; North et al., 2020). In particular, inhibition of topoisomerases II by BZ metabolites and subsequent chromosomal damage, alteration of cell signaling pathways, and immune-mediated bone marrow dysfunctions have been reported (Frantz et al., 1996; Lindsey et al., 2004; Sauer et al., 2018; Duval et al., 2019; Lu et al., 2020; North et al., 2020). Increasing evidence indicates that BZ induces epigenetic changes, leading to aberrant DNA and histone methylation, and that epigenetic alterations contribute to BZ-dependent leukemogenesis (Smith, 2010; Chappell et al., 2016; Fenga et al., 2016; Yu et al., 2019; Chung and Herceg, 2020). Interestingly, normal and malignant hematopoiesis is known to rely on epigenetic processes such as histone modifications (Butler and Dent, 2013; Chopra and Bohlander, 2015). As such, epigenetic enzymes, notably histone methyltransferases, are recurrently mutated and dysregulated in hematologic malignancies (Butler and Dent, 2013; Husmann and Gozani, 2019).

The histone mark H3K36me3 is a key epigenetic modification that is linked to transcription, alternative splicing, and DNA repair (Wagner and Carpenter, 2012; Li et al., 2016; Fahey and Davis, 2017; Husmann and Gozani, 2019). The nonredundant histone methyltransferase SETD2 is the sole methyltransferase that mediates trimethylation of H3K36 to generate H3K36me3 (Edmunds et al., 2008; Husmann and Gozani, 2019). Recurrent SETD2-inactivating mutations and altered H3K36me3 levels are found in cancer at a high frequency, and several studies suggest that SETD2 acts as a tumor suppressor (Kudithipudi and Jeltsch, 2014; Fahey and Davis, 2017; Husmann and Gozani, 2019). Importantly, SETD2 and the H3K36me3 mark play a crucial role in hematopoiesis (Wang et al., 2018; Zhang et al., 2018; Zhou et al., 2018; Chen et al., 2020). Accordingly, loss-of-function mutations in SETD2 and subsequent aberrant H3K36 trimethylation are among the most common alterations found in blood malignancies, supporting that disruption of the SETD2-dependent H3K36me3 mark contributes to malignant hematopoiesis (Huether et al., 2014; Mar et al., 2014, 2017; Zhu et al., 2014; Dong et al., 2019). Using molecular and cellular approaches, we provide here mechanistic evidence that human SETD2 is inactivated by BQ, leading to reduced levels of H3K36me3. More specifically, we found that loss of SETD2 methyltransferase activity is due to covalent binding of BQ to cysteine residues within the catalytic domain of SETD2, in particular Zn^{2+}-bound cysteines located in the AWS zinc finger. We also observed that generation of BQ-SETD2 quinoproteins also resulted in the formation of SETD2 crosslinks/oligomers, in agreement with the aggregation-prone properties of SETD2 and previous studies with other enzymes (Shu et al., 2019, 2020a). Taken together, our data suggest that the hematotoxic metabolite of BZ, 1,4-benzoquinone, may contribute to BZ-dependent leukemogenesis by altering the activity of the H3K36 methyltransferase SETD2. More broadly, our work provides molecular and cellular evidence that certain hematotoxic metabolites of benzene could directly impact epigenetic processes of hematopoietic relevance.

Materials and Methods

Chemicals and Reagents. Antibodies used in this paper are as follows: H3K36me3 (ab9050; Abcam), SETD2 (PA5-34934; ThermoFisher), 6× histidine-tag (H1029; Sigma-Aldrich, France), GFP-tag (B2; Santa Cruz), plumbagin [kind gift of Dr. Hiroyuki Tanaka (Kyushu University)], H3 (3638S; Cell Signaling, France), γ-H2AX (CR55T33; eBioscience), secondary anti-rabbit (A1949; Sigma-Aldrich), and secondary anti-mouse (31430; ThermoFisher). 1,4-Benzoquinone, hydroquinone, phenol, benzene, plumbagin, nitro blue tetrazolium, iodoacetamide-fluorescein, *S*-adenosylmethionine, 4-(2-pyridylazo)resorcinol, *N*,*N*,*N*′,*N*′-tetrakis(2-pyridinylmethyl)-1,2-ethanediamine, *N*-ethylmaleimide, dithiothreitol, dimethylsulfoxide, β-mercaptoethanol, His-select nickel resin, protease inhibitors, lysozyme, isopropyl β-D-1-thiogalactopyranoside, formaldehyde, Triton X-100, and horseradish peroxidase were from Sigma-Aldrich (France). pET28-MHL SETD2 (1435–1711) plasmid was from Addgene (40741), and GFP-SETD2 (500-2564) plasmid was a kind gift of Dr. Sérgio De Almeida (Faculdade de Medicina da Universidade de Lisboa). PD-10 desalting column was from GE Healthcare (52-1308-00), protein A-agarose and G-agarose were from Santa Cruz (sc2001 and sc-2002), Metafectene was from Biontex, and Bradford reagent was from Bio-Rad. H3K36 peptide (5-FAM-TGGVKRPHR-NH_2) and its methylated form, H3K36me (5-FAM-TGGVK_{me}RPHR-NH_2), were from Proteogenix. 1,4-Benzoquinone, hydroquinone, phenol, benzene, and plumbagin were diluted in DMSO at a stock concentration of 150 mM.

Recombinant Protein Expression and Purification. cDNA sequence from human SETD2 encoding for the AWS domain (residues 1494–1550) was cloned into pET28a expression vector. pET28-MHL SETD2 and pET28a AWS domain were transformed into HI-Control BL21 (DE3) *Escherichia coli*, and bacteria were grown in Luria-Broth medium at 37°C under agitation until reaching an optical density of 0.6. Protein expression was then induced by adding 750 μM isopropyl β-D-1-thiogalactopyranoside and lowering the temperature to 16°C overnight under agitation. Cells were pelleted and resuspended in lysis buffer (PBS, pH 8, 300 mM NaCl, 1% Triton X-100, 1 mg/ml lysozyme and protease inhibitors) for 30 minutes at 4°C. The resulting lysate was sonicated (10 minutes, 10 seconds ON, 20 seconds OFF, 20% power) and clarified by centrifugation (15000*g*, 30 minutes, 4°C). The supernatant was then incubated for 2 hours on ice in the presence of 10 mM imidazole and 1 ml His-select nickel resin under agitation. Beads were loaded on a column equilibrated with PBS, pH 8, and 300 mM NaCl and washed with washing buffer (PBS, pH 8, 300 mM NaCl, 0.1% Triton X-100) followed by a second wash with washing buffer without Triton X-100. Protein was eluted using elution buffer (PBS, pH 8, 300 mM NaCl, and 300 mM imidazole), and highly concentrated fractions were pooled and incubated on ice for 30 minutes in the presence of 10 mM dithiothreitol (DTT). Purified proteins were buffer-exchanged using PD-10 desalting columns to methyltransferase buffer (50 mM Tris-HCl, 50 mM NaCl, pH 8), and its purity was determined by SDS-PAGE and Coomassie

ABBREVIATIONS: AWS, associated with SET; BQ, 1,4-benzoquinone; BZ, benzene; CDK2, Cyclin-Dependent Kinase 2; ChIP, chromatin immunoprecipitation; Ctrl, control; DAPI, 4′,6-diamidino-2-phenylindole; DTT, dithiothreitol; FA, formic acid; GFP, green fluorescent protein; H3K36, lysine 36 of histone H3; H3K36me3, trimethylated histone H3 lysine 36; IAF, iodoacetamide-fluorescein; MYC, Myelocytomatosis; NBT, nitroblue tetrazolium; NEM, *N*-ethylmaleimide; PAR, 4-(2-pyridylazo)resorcinol; PBG, plumbagin; PH, phenol; PO, peroxidase; qPCR, quantitative polymerase chain reaction; SAM, *S*-adenosylmethionine; SET, Su(var)3-9, Enhancer-of-zeste and Trithorax; SETD2, SET domain containing 2; UFLC, ultra-fast liquid chromatography system.

staining. Proteins were kept at –80°C. Before use, recombinant SETD2 or AWS domain were incubated in the presence of 2 mM DTT for 15 minutes on ice. Proteins were then buffer-exchanged using PD-10 desalting columns to methyltransferase buffer, and protein concentration was assessed by Bradford assay.

UFLC-Mediated SETD2 Methyltransferase Activity Assay. The H3K36 methyltransferase activity of SETD2 was determined as previously described (Duval et al., 2015). Recombinant SETD2 was incubated with 75 μM H3K36 peptide and 75 μM *S*-adenosylmethionine (SAM) in 50 μl of methyltransferase buffer overnight at room temperature. Reaction was then stopped with the addition of 50 μl perchloric acid ($HClO_4$) (15% v/v in water), and 10-μl aliquots of the mixture were injected in a reverse phase ultra-fast liquid chromatography system (UFLC) (Shimadzu, France). The mobile phase used for the separation consisted of two solvents: A was water with 0.1% $HClO_4$, and B was acetonitrile with 0.1% trifluoroacetic acid. Separation was performed by an isocratic flow (80% A/20% B) rate of 1 ml/min on a Kromasil column 100-5-C18 (4.6 × 250 mm at 40°C). H3K36 peptide (substrate) and its methylated form (H3K36me, product) were monitored by fluorescence emission (λ= 530 nm) after excitation at λ= 485 nm and quantified by integration of the peak fluorescence area.

Effects of Benzene and Benzene Metabolites on SETD2 Activity. Recombinant SETD2 (3 μM) was incubated with increasing concentrations of benzene (BZ), phenol (PH), hydroquinone (HQ) (25, 50, 100 μM), BQ (3, 6, 12 μM), or vehicle (Ctrl) for 10 minutes at room temperature. In total, 10 μl of the mixture was then diluted with 40 μl methyltransferase buffer containing 75 μM H3K36 peptide and 75 μM SAM (final concentrations). SETD2 H3K36 methyltransferase activity was assayed overnight at room temperature and was assessed by UFLC as described above.

Determination of SETD2 H3K36 Methyltransferase Activity on Core Histone Substrates. Recombinant SETD2 (3 μM) was incubated with 30 μM BZ, PH, HQ, BQ, or vehicle (Ctrl) for 10 minutes at room temperature in methyltransferase buffer. In total, 10 μl of the mixture was then diluted with 10 μl methyltransferase buffer containing 1 μg purified human core histones [from SETD2-KO HEK293 cells (Hacker et al., 2016)] and 100 μM SAM (final concentrations) and incubated overnight at room temperature. Samples were then separated by SDS-PAGE (18% gel) and transferred onto a nitrocellulose membrane. SETD2-dependent methylation of H3K36 was detected using an anti H3K36me3 antibody. Ponceau staining was used to ensure equal protein loading.

Effects of Buffer Exchange and DTT Reducing Agent on BQ-Inactivated SETD2. To test the effect of buffer exchange on BQ-inactivated SETD2, recombinant SETD2 (3 μM) was incubated with 30 μM BQ or vehicle (Ctrl) for 10 minutes at room temperature in methyltransferase buffer. Samples were then buffer-exchanged using a PD-10 column to methyltransferase buffer. SETD2 H3K36 methyltransferase activity was assessed by UFLC as described above.

To test the effect of dithiothreitol (DTT) on BQ-inactivated SETD2, recombinant SETD2 (3 μM) was incubated with 30 μM BQ or vehicle (Ctrl) for 10 minutes at room temperature, followed by a second incubation in the presence of 10 mM DTT for 10 minutes at room temperature in methyltransferase buffer. SETD2 H3K36 methyltransferase activity was assessed by UFLC as described above.

Detection of Quinoprotein Adducts by Nitroblue Tetrazolium. Detection of quinone-protein adducts were carried out using the nitroblue tetrazolium (NBT) method as reported previously (Shu et al., 2019). Briefly, recombinant SETD2 (5 μg) or recombinant AWS domain (5 μg) were incubated with increasing concentration of BQ (7, 15, 30 μM), plumbagin (PBG; 30 μM), or vehicle (Ctrl) for 10 minutes (BQ) or 15 minutes (PBG) at room temperature in methyltransferase buffer. Reactions were stopped with the addition of Laemmli sample buffer containing 400 mM β-mercaptoethanol, and samples were separated by SDS-PAGE and transferred onto a nitrocellulose membrane. Membrane was then incubated with a solution of 2 M potassium glycinate, 0.6 mg/ml NBT (pH 10.0) at room temperature for 45 minutes in the dark. Upon purple precipitate apparition, membrane was further blocked with 5% nonfat milk in phosphate buffer containing 1% Tween-20 (PBST) for 1 hour at room temperature and later used for immunodetection of SETD2 protein or ponceau staining.

Labeling of Free Cysteine Residues Using Iodoacetamide-Fluorescein. Labeling of free cysteine residues with iodoacetamide-fluorescein (IAF) was carried out as reported previously (Duval et al., 2019). Recombinant SETD2 (5 μg) or recombinant AWS domain (5 μg) were incubated in the increasing concentration of BQ (0, 7, 15, 30 μM), PBG (30 μM), or vehicle (Ctrl) for 10 minutes (BQ) or 15 minutes (PBG) at room temperature in methyltransferase buffer. In total, 20 μM IAF was added to the mixture, and samples were further incubated for 15 minutes at 37°C. Reactions were stopped by the addition of Laemmli sample buffer containing 400 mM β-mercaptoethanol, and samples were separated by SDS-PAGE and transferred onto a nitrocellulose membrane. IAF fluorescence on labeled cysteine residues was detected using a Fujifilm LAS 4000 detection system (λ_{exc} = 485 nm, λ_{em} = 530 nm). A ponceau staining of the membrane was done to ensure equal protein loadings.

Kinetics of SETD2 Inactivation by 1,4-Benzoquinone. Recombinant SETD2 (5 μM) was incubated with increasing concentrations of BQ (0, 20, 30, 40 μM) on ice in methyltransferase buffer. Every 30 seconds, an aliquot of the mixture was taken and diluted 10 times, and SETD2 residual activity was measured by UFLC as described above. Data were analyzed as described previously for irreversible inhibitors under pseudo first-order conditions using OriginPro software (version 2021; OriginLab Corporation, Northampton, MA) (Copeland, 2005). The equation rate of inhibition of SETD2 by BQ can be represented as follows: Ln (% residual SETD2 activity) = $-k_{obs} \times t$, where k_{obs} is apparent first-order inhibition rate constant, and t is time. For each BQ concentration, the k_{obs} values were extracted from the slopes of the natural logarithm of the percentage of SETD2 activity as a function of time. The second-order rate constant (k_{inact}) was obtained from the slope of k_{obs} values plotted as a function of BQ concentration ($k_{inact} = k_{obs}/[BQ]$).

PAR-Mediated Zn^{2+} Release Analysis. Recombinant SETD2 (5 μg) or recombinant AWS domain (5 μg) were incubated with 30 μM BZ, PH, HQ, BQ, PBG, 1 mM *N*-ethylmaleimide (NEM) or vehicle (Ctrl) in the presence of 100 μM 4-(2-pyridylazo)resorcinol (PAR) for 20 minutes at room temperature in methyltransferase buffer. PAR reacts with free Zn^{2+} in solution according to the following equation:

$$2\text{PAR} + Zn^{2+} \rightarrow \text{PAR(2)-}Zn^{2+}.$$

The orange-colored complex PAR(2)-Zn^{2+} has an absorption peak at 490 nm. The reaction was started by the addition of benzene, benzene metabolites, PBG, or NEM and was monitored by reading the absorbance of the solution every minute at 490 nm using a microplate reader (Biotek Instruments, France).

Mass Spectrometry Analysis of Plumbagin Adducts. Recombinant SETD2 catalytic domain or AWS Zn-finger domain (3 μM) were incubated with 60 μM PBG for 30 minutes at room temperature in assay buffer. The reaction was stopped with 10 mM DTT and diluted 10 times in methyltransferase buffer, and unmodified cysteines were blocked by addition of 10 mM *N*-ethylmaleimide for 10 minutes. Samples were then incubated overnight at 37°C with trypsin (Promega, France) at 12.5 ng/μl in 25 mM ammonium bicarbonate (pH 8.0). The supernatant containing peptides was acidified with formic acid (FA), desalted on C18 tips (Pierce C18 tips, Thermo Scientific, France), and eluted in 10 μl 70% ACN, 0.1% FA. Desalted samples were evaporated using a SpeedVac and then taken up in 10 μl of buffer A (water, 0.1% FA), and 5 μl was injected on a nanoLC High performance liquid chromatography (HPLC) system (Thermo Scientific, France) coupled to a hybrid quadrupole-Orbitrap mass spectrometer (Thermo Scientific, France). Peptides were loaded on a reverse phase C18 μ-precolumn (C18 PepMap100, 5 μm, 100 A, 300 μm i.d. × 5 mm) and separated on a C18 column (EASY-spray C18 column, 75 μm i.d. × 50 cm) at a constant flow rate of 300 nl/min

with a 120-minute gradient of 2% to 40% buffer B (buffer B: 20% water, 80% ACN, 0.1% FA). Mass spectrometry (MS) analyses were performed by the Orbitrap cell with a resolution of 120.000 [at m/z (mass number/charge number) 200]. Tandem mass spectrometry (MS/MS) fragments were obtained by Higher-energy C-trap dissociation (HCD) activation (collisional energy of 28%) and acquired in the ion trap in top-speed mode with a total cycle of 3 seconds. The database search was performed against the Swissprot database and the *Homo sapiens* taxonomy with Mascot version 2.5.1 software with the following parameters: tryptic peptides only with up to two missed cleavages, variable modifications: cysteine plumbagin and methionine oxidation. MS and MS/MS error tolerances were set respectively to 7 ppm and 0.5 Da. Peptide identifications were validated using a 1% false discovery rate threshold obtained by Proteome Discoverer (version 2.2; Thermo Scientific, France) and the percolator algorithm. The candidate sequences modified by plumbagin were manually inspected for de novo sequencing.

Bioactivation of HQ into BQ Using Peroxidase Hydroquinone-Bioactivation System. Bioactivation of HQ into BQ by peroxidase (PO) was carried out as previously described (Eastmond et al., 2005). Horseradish PO (0.03 mg/ml) was incubated in the presence of hydroquinone (300 μM) and H_2O_2 (50 μM) for 30 minutes at room temperature in methyltransferase buffer. Heat-inactivated PO (100°C, 30 minutes) was used as a negative bioactivation control. Conversion of HQ to BQ was assessed by spectrophotometry (UV-1650PC; Shimadzu, France) by reading the absorbance spectrum of the solution between 220 and 340 nm. Recombinant SETD2 (3 μM) was then incubated with a 1:10 dilution of the previous bioactivation mixture for 10 minutes at room temperature in methyltransferase buffer. Residual SETD2 H3K36 methyltransferase activity was assessed by UFLC as described above.

Western Blotting. Samples were separated by SDS-PAGE followed by a transfer onto a nitrocellulose membrane (0.22 μm, GE Healthcare) for 1 hour at 4°C. Membranes were blocked in 5% nonfat milk in PBS 0.1% Tween-20 (PBST) for 1 hour and incubated overnight with primary antibody in 1% nonfat milk PBST at 4°C. The next day, membranes were washed three times with PBST prior to incubation with secondary antibody for 1 hour at room temperature. Membranes were then washed three more times, and the signal was detected by chemiluminescence using Enhanced Chemiluminescence (ECL) Prime reagent (GE Healthcare) on an Amersham Imager 600 detection system (GE Healthcare, France).

Cell Culture, Transfection of HEK293T Cells, and Cell Treatment. HEK293T, K562, and HeLa cells were grown in RPMI 1640 medium with 10% heat-inactivated FBS and 1 mM L-glutamine at 37°C under 5% CO_2. Human CD34+ cells (from a healthy human donor) were maintained in RPMI 1640 medium with 20% heat-inactivated FBS, penicillin (100 U/ml), streptomycin (100 μg/ml), and 1 mM L-glutamine at 37°C under 5% CO_2. Cells were routinely tested for mycoplasma using DAPI staining. For transfection, HEK293T cells were seeded at 30,000 cells/cm^2 in a 100-cm^2 Petri dish and directly transfected using a solution containing 9 μg of GFP-SETD2 plasmid and 18 μl metafectene. Cells were then put back in the incubator at 37°C and 5% CO_2 for 48 hours.

For 1,4-benzoquinone treatment, K562, CD34+, and HeLa cells (10×10^6) were exposed to BQ or vehicle (Ctrl) for 30 minutes at 37°C, 5% CO_2, in RPMI 1640 medium and then put back in the incubator for 3 more hours (6 hours for HeLa) at 37°C, 5% CO_2, in RPMI 1640 medium. BQ concentrations used were 0, 1, 2, 5, and 10 μM for K562 cells; 10 μM for CD34+ cells; and 20 μM for HeLa cells.

Immunofluorescence Detection of SETD2 in BQ-Treated HeLa Cells. HeLa cells (10×10^6) were fixed on slides using methanol at −20°C for 20 minutes. Methanol was then evaporated, and the slides were dried for 10 minutes. Cells were permeabilized with a PBS solution containing 0.1% Triton X-100 for 10 minutes at room temperature and washed three times with PBS before being incubated overnight with SETD2 (1:1000) and γ-H2AX (1:2000) antibodies in PBST at 4°C. After three washes in PBS, the slides were incubated for 45 minutes at room temperature in PBST containing a suitable secondary antibody α-rabbit (Alexa Fluor 488, 1:500) or α-mouse (Alexa Fluor 594, 1:500). The slides were then washed with PBS, mounted, and marked with DAPI (Flourshield).

Acid Extraction of Endogenous Histones. Treated K562 cells were lysed using cell lysis buffer (PBS 150 mM NaCl, pH 7.5, 1% Triton X-100, protease inhibitors) for 30 minutes at 4°C under agitation. The lysate was sonicated for 2 seconds (10% power) and then centrifuged for 15 minutes at 15,000*g* (4°C). The soluble fraction corresponds to total protein cell extract, and the pellet corresponds to insoluble chromatin and membranes. Total protein cell extracts were kept to be further used in Western blot analysis, and pellets were further incubated overnight in the presence of 0.2 N HCl at 4°C under agitation. The next day, the acid extracted histones were centrifugated for 15 minutes at 15,000*g* (4°C), and the supernatant containing the extracted histones was kept. Histone concentrations were determined using Bradford assay. In total, 2.5 μg of extracted histones were separated by SDS-PAGE (18% gel) and transferred onto a nitrocellulose membrane. SETD2-dependent methylation of H3K36 was detected using an anti-H3K36me3 antibody. A ponceau staining of the membrane was done to ensure equal protein loading.

Treatment of Cell Extracts and Immunoprecipitation of GFP-SETD2. GFP-SETD2–transfected HEK293T cells were lysed using cell lysis buffer (PBS 150 mM NaCl, pH 7.5, 1% Triton X-100, protease inhibitors) for 30 minutes at 4°C under agitation. The lysate was sonicated for 2 seconds (10% power) and then centrifuged for 15 minutes at 15,000*g* (4°C). In all, 1 mg of total protein extract (soluble fraction) was incubated with increasing concentrations of BQ (0, 25, 50 μM) or vehicle (Ctrl) for 30 minutes on ice and further incubated overnight at 4°C with 1.5 μg anti-GFP antibody and protease inhibitors under agitation. The following day, samples were rocked for 2 more hours at 4°C with 30 μl protein G-agarose. Beads were then washed three times with cell lysis buffer and two times with methyltransferase buffer and split in two: one-fifth of the beads was mixed with 20 μl Laemmli sample buffer containing 400 mM β-mercaptoethanol to be further used in Western blot analysis, and the rest was incubated with 30 μl methyltransferase buffer containing 75 μM H3K36 peptide, 75 μM SAM, 1 mM DTT, and protease inhibitors overnight at room temperature. The reaction was then stopped with the addition of 50 μl perchloric acid ($HClO_4$) (15% v/v in water), and SETD2 H3K36 methyltransferase activity was assessed by UFLC as described above.

Chromatin Immunoprecipitation of BQ-Treated K562 Cells. K562 cells (10×10^6) were fixed with 1% formaldehyde for 10 minutes at 37°C. The reaction was stopped with the addition of 0.125 M glycine for 5 minutes at 4°C. Cells were then proceeded for chromatin immunoprecipitation (ChIP) using True Microchip kit (Diagenode SA) according to the manufacturer's instructions. DNA was immunoprecipitated using H3K36me3 and H3 (positive control) antibodies. Rabbit IgG was also used as a negative control. Immunocomplexes were isolated with protein A-agarose beads. DNA was isolated using the MicroChIP DiaPure columns (Diagenode SA). The primers used for qPCR were from Hacker et al. (2016) and correspond to *MYC* exon 2 and *CDK2* exon 6.

Human MYC_F: TGCCCCTCAACGTTAGCTTC
Human MYC_R: GGCTGCACCGAGTCGTAGTC
Human CDK2_F: CCCTATTCCCTGGAGATTCTG
Human CDK2_R: CTCCGTCCATCTTCATCCAG

Fold enrichments of ChIP experiments were calculated by comparing the H3K36me3 ChIP with the IgG control and then normalized to the H3 antibody internal control of ChIP quality.

Statistical Analysis. The experiments carried out in this manuscript have not been designed to address a specific quantifiable statistical null hypothesis and thus have an exploratory character. The computed *P* values are therefore only descriptive. Values are presented as means ± S.D. of three independent experiments and analyzed by either *t* test or one-way ANOVA using Rstudio [R Core Team (2017); R Foundation for Statistical Computing, Vienna, Austria] or Prism GraphPad 5 (GraphPad Prism version 5.0.0 for Windows; GraphPad

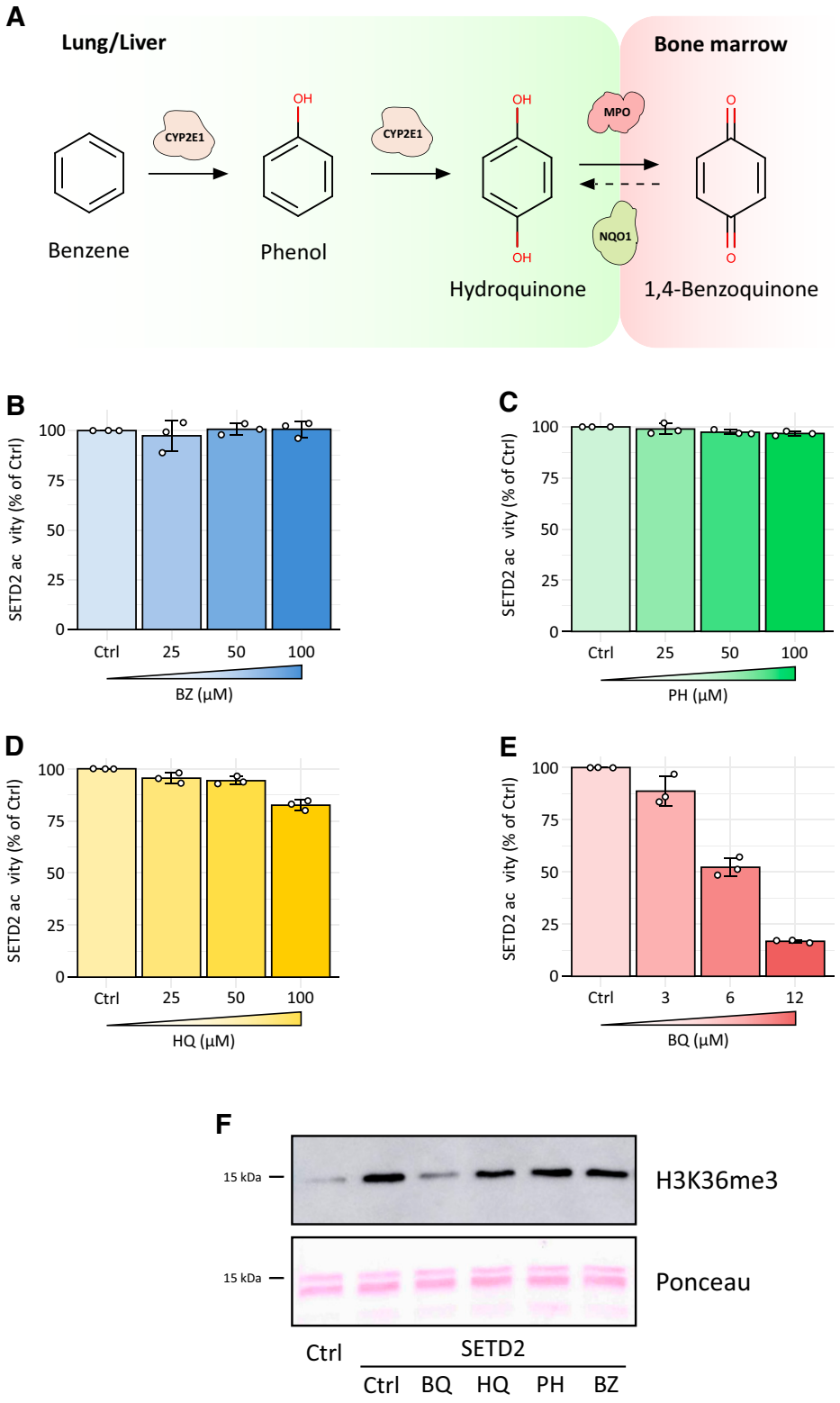

Fig. 1. Inhibition of the histone methyltransferase activity of human SETD2 by BZ, PH, HQ, and BQ. (A) Schematic representation of BZ bioactivation into BQ in bone marrow. MPO: myeloperoxidase; NQO1: NAD(P)H Quinone Dehydrogenase 1. (B–E) Recombinant SETD2 (3 µM) was incubated with increasing concentrations of BZ (B, 0–100 µM), PH (C, 0–100 µM), HQ (D, 0–100 µM), or BQ (E, 0–12 µM) for 10 minutes at room temperature. SETD2 residual activity was measured by UFLC using a H3K36 fluorescent peptide. Bar plots and error bars represent the means and the S.D. of three independent experiments. (F) SETD2 was incubated in the presence of 30 µM BZ, PH, HQ, or BQ for 10 minutes at room temperature. Residual SETD2 methyltransferase activity was assessed by incubating the enzyme with purified human core histones and detection of the H3K36me3 histone mark on nitrocellulose membranes using a specific antibody. Ponceau staining was carried out to ensure equivalent protein loading.

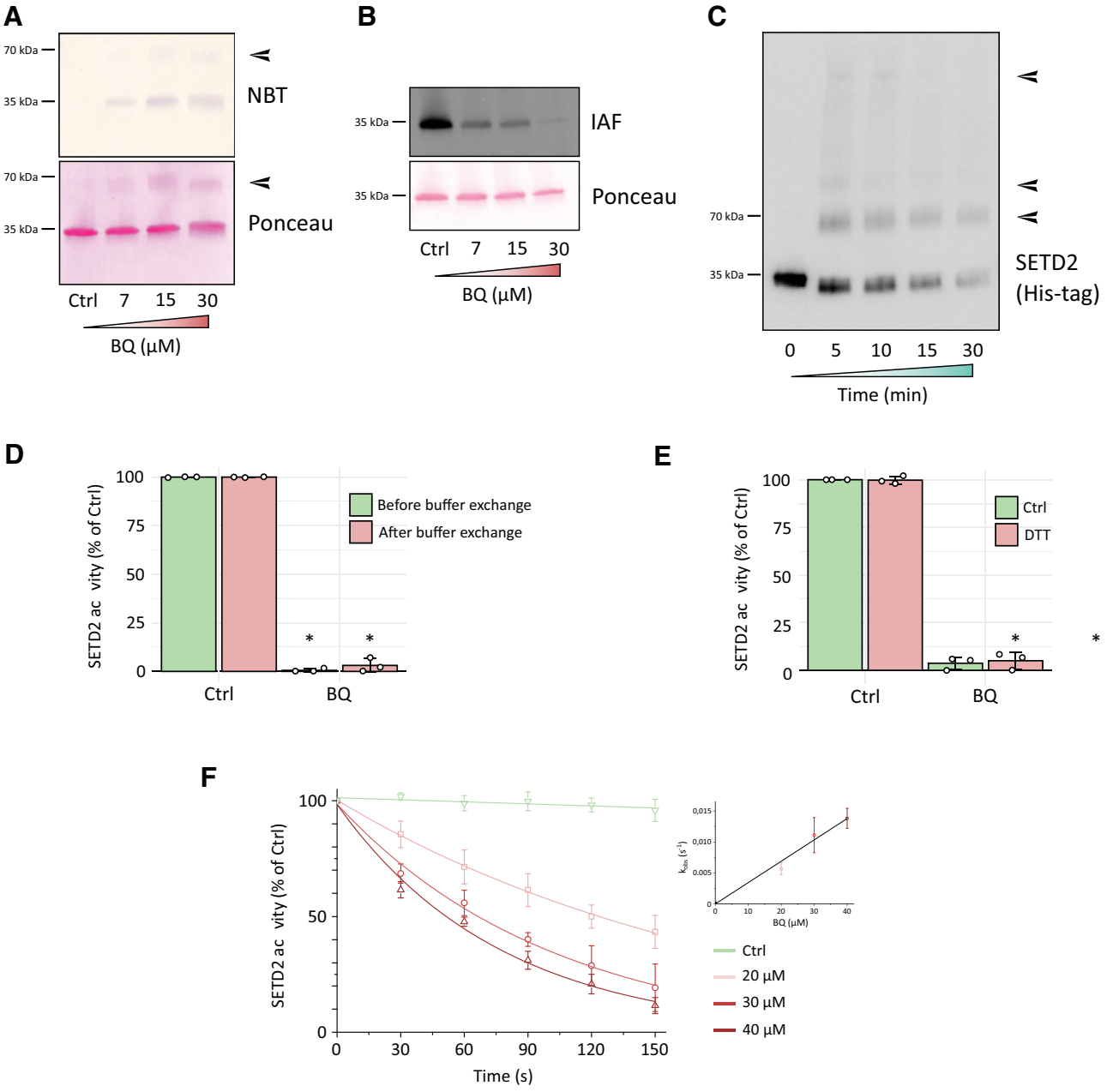

Fig. 2. BQ forms covalent adducts with SETD2 cysteine residues and protein crosslinks/oligomers. (A) The Benzene Hematotoxic and Reactive Metabolite 1,4-Benzoquinone Impairs the Activity of the Histone Methyltransferase SET Domain Containing 2 (SETD2) and Causes Aberrant Histone H3 Lysine 36 Trimethylation (H3K36me3). (B) Recombinant SETD2 was incubated with increasing concentrations of BQ (0–30 μM) for 10 minutes at room temperature, followed by a second incubation with 20 μM IAF for 10 minutes at 37°C. Samples were then separated by SDS-PAGE and transferred onto a nitrocellulose membrane. IAF-labeled cysteine residues were detected by fluorescence emission (λ_{exc} = 485 nm, λ_{em} = 530 nm). Ponceau staining was carried out to ensure equal protein loading. (C) Recombinant SETD2 was incubated with 30 μM BQ at room temperature. At different time points, an aliquot of the mixture was taken and diluted into Laemmli buffer containing 400 mM β-mercaptoethanol. Samples were then separated by SDS-PAGE and transferred onto a nitrocellulose membrane. SETD2 was detected using an antibody against 6× Histidine-tag. Black arrows represent high-molecular-weight SETD2 protein crosslinks/olig omers. (D) Recombinant SETD2 was incubated with 30 μM BQ for 10 minutes at room temperature and buffer-exchanged using PD-10 columns into methyltransferase buffer (see *Materials and Methods*). Residual SETD2 activity was measured by UFLC using a H3K36 fluorescent peptide. Bar plots and error bars represent the means and the S.D. of three independent experiments, respectively. *$P < 0.05$ compared with Ctrl. (E) Recombinant SETD2 was preincubated with 30 μM BQ for 10 minutes at room temperature, followed by an incubation with 10 mM DTT for 10 minutes at room temperature. Residual SETD2 was measured by UFLC using a H3K36 fluorescent peptide. Bar plots and error bars represent the means and the S.D. of three independent experiments, respectively. *$P < 0.05$ compared with Ctrl. (F) Recombinant SETD2 was incubated with increasing concentrations of BQ (0–40 μM) on ice. Every 30 seconds, an aliquot of the mixture was taken and diluted 10 times, and residual SETD2 activity was measured by UFLC using a H3K36 fluorescent peptide. For each BQ concentration, the percentage (%) of SETD2 residual activity was plotted as a function of time. The apparent first-order inhibition constants (k_{obs}) were calculated from the slope of the natural logarithm–based linear regression of the previous representation (see *Material and Methods*). The k_{obs} values were then plotted against BQ concentrations, and the second-order inhibition constant (k_{inact}) was extracted from the slope (inset). Dot plots and error bars represent the means and the S.D. of three independent experiments, respectively.

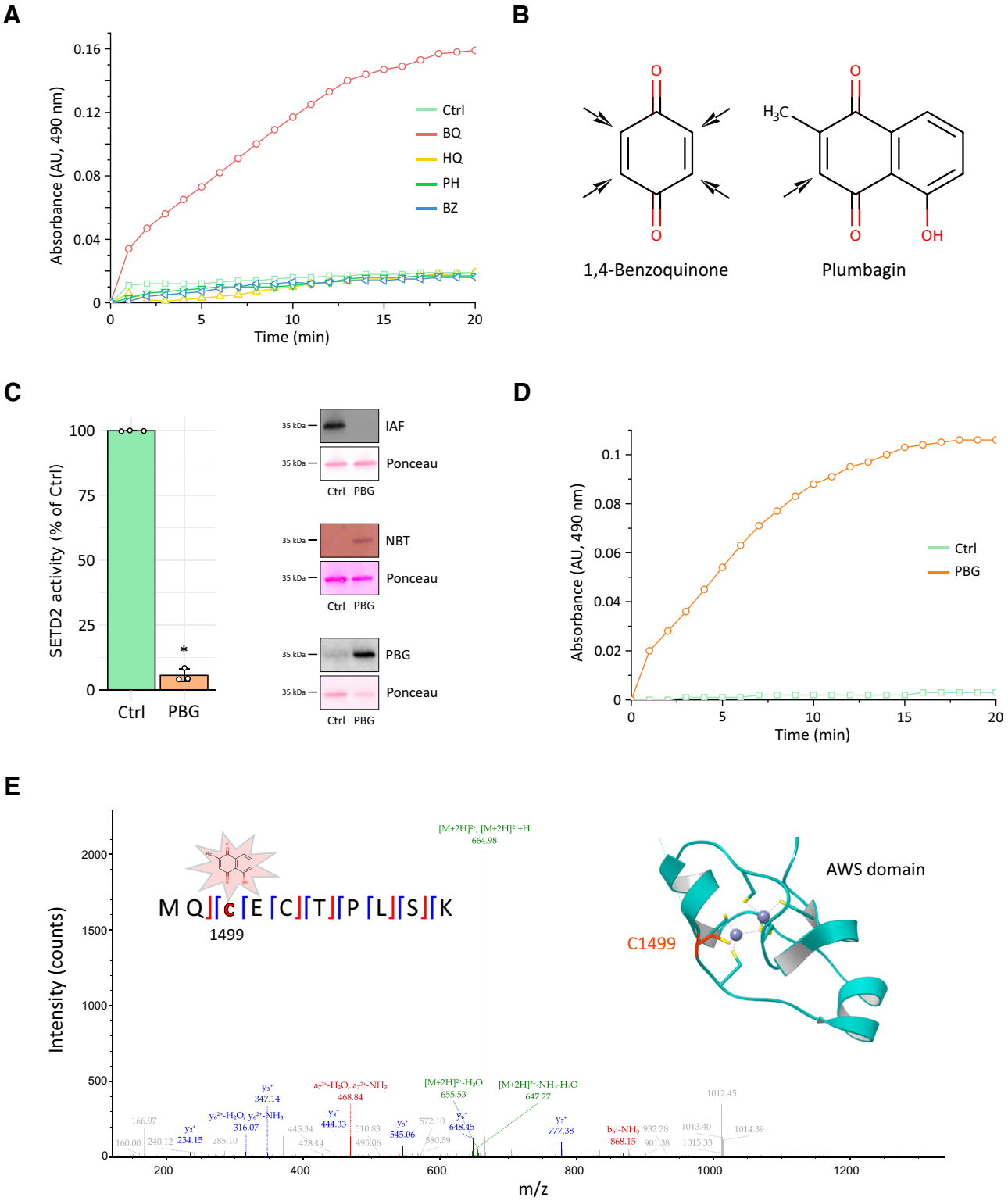

Fig. 3. BQ reacts with zinc-finger cysteine residues within the AWS domain of SETD2, leading to zinc release. (A) Recombinant SETD2 was incubated with 30 μM BZ, PH, HQ, or BQ and 100 μM PAR for 20 minutes at room temperature. The absorbance of PAR-Zn^2 complexes (490 nm) was followed every minute using a plate reader. (B) Comparison of the chemical structures of BQ and PBG. Black arrows represent potential Michael adduction sites. (C) Left panel: recombinant SETD2 was incubated in the presence of 30 μM PBG for 15 minutes at room temperature. Residual SETD2 activity was then measured by UFLC using a H3K36 fluorescent peptide. Bar plots and error bars represent the means and the S.D. of three independent experiments, respectively. *$P < 0.05$ compared with Ctrl. Right panel: recombinant SETD2 was incubated with 30 μM PBG for 15 minutes at room temperature. For the NBT staining of quinoprotein adducts, samples were then separated by SDS-PAGE and transferred onto a nitrocellulose membrane. Plumbagin adducts on SETD2 were then detected using NBT staining as described in *Materials and Methods*. For the IAF cysteine labeling, samples were incubated with 20 μM IAF for 10 minutes at 37°C, separated by SDS-PAGE, and transferred onto a nitrocellulose membrane. IAF-labeled cysteine residues were detected by fluorescence emission (λ_{exc} = 485 nm, λ_{em} = 530 nm). For the

Software, San Diego, CA) followed by two-tailed Dunnett's test. $P < 0.05$ was used to consider differences as statistically significant.

Results

BQ Inhibits SETD2 H3K36 Methyltransferase Activity. BZ is known to be readily biotransformed into oxidative metabolites in bone marrow cells (Fig. 1A) (Smith, 2010). We tested the effects of BZ and its major oxidative metabolites on SETD2 catalytic domain (residues 1435–1711). As shown in Fig. 1, B–E, the H3K36 methyltransferase activity of SETD2 was significantly inactivated by low micromolar concentrations of BQ ($IC_{50} \approx 6$ μM). Conversely, no or very modest effects of phenol or hydroquinone were observed at concentrations up to 100 μM. Moreover, BQ generated from hydroquinone by an in vitro peroxidase/H_2O_2 system that mimics the formation of BQ in bone marrow was able to completely inactivate SETD2, thus further underlining the reactivity of this BZ metabolite toward SETD2 (Frantz et al., 1996) (Supplemental Fig. 1). The levels of BQ in bone marrow tissues upon BZ exposure have not been reported. However, different studies indicate that metabolites of BZ (including PH and HQ) could reach high micromolar concentrations (≈180 μM/ppm of BZ) (Kim et al., 2006b; Rappaport et al., 2010). Levels of HQ (the precursor of BQ) close to 50 μM have been measured in urine of workers exposed to BZ (Kim et al., 2006a). Histone methyltransferase assays conducted with purified core histones confirmed that BQ was the sole BZ metabolite able to impair the trimethylation of H3K36 by SETD2 (Fig. 1F).

BQ Forms Michael Adducts on Active Site Zinc-Finger Cysteines and Impairs Irreversibly SETD2 Histone Methyltransferase Activity. BQ is known to be capable of reacting with certain redox-sensitive cysteines forming covalent quinone-thiol Michael adducts (Shu et al., 2019). As shown in Fig. 2, A and B, NBT redox staining and free cysteine labeling with IAF supported the formation of BQ-protein adducts on cysteines within the catalytic domain of SETD2. We also found that BQ led to the formation of non-reducible SETD2 protein crosslinks/oligomers as previously observed for other enzymes inhibited by BQ (Fig. 2, A and C) (Shu et al., 2020a, 2020b). Interestingly, SETD2 has been shown to be inherently prone to protein crosslink/aggregation, which can be detected by SDS-PAGE/Western blot or immunofluorescence (Bhattacharya and Workman, 2020). We found that the activity of SETD2 could not be restored by buffer exchange or reduction by DTT, which is consistent with the formation of irreversible cysteine-BQ adducts and protein crosslinks/oligomers (Fig. 2, D and E). Moreover, the inactivation of SETD2 by BQ was concentration- and time-dependent, with a second-order inhibition rate constant (k_i) equal to 4×10^2 $M^{-1} \cdot second^{-1}$, thus further supporting the irreversible nature of the inactivation (Fig. 2F).

Cysteine residues are chemically and kinetically favored sites for BQ adduction, and as such, certain enzymes can be impaired by formation of BQ adducts on reactive cysteines (Bender et al., 2007; Mbiya et al., 2013; Duval et al., 2019; Shu et al., 2020b). SETD2 catalytic domain possesses two Zn-finger regions (AWS and SET/post-SET) containing three Zn atoms chelated by cysteines that contribute to the folding of the domain and ensure enzyme function (Yang et al., 2016; Zhang et al., 2017) (Supplemental Fig. 2A). Moreover, electrophilic agents such as BQ can react with certain reactive Zn-bound cysteines in Zn-fingers causing Zn ejection and protein unfolding (Lee et al., 2013). In agreement with this, we observed that BQ (but not BZ or the other BZ metabolites) was able to cause Zn release from SETD2 catalytic domain (Fig. 3A). Mass spectrometry experiments were carried out to identify the cysteines adducted by BQ. However, in initial attempts, no individual amino acid residues were identified. This is likely due to the ability of BQ to crosslink multiple residues in SETD2, as observed previously for topoisomerase IIα (Bender et al., 2007). To circumvent this technical difficulty, plumbagin (a quinone that has one single reactive site for adduction) was used as a surrogate of BQ as previously described by Bender et al. (2007) (Fig. 3B). As observed with BQ, we confirmed that PBG formed covalent adducts with cysteine residues within SETD2 catalytic domain with concomitant loss of enzyme activity and Zn release (Fig. 3, C and D). Mass spectrometry analysis confirmed the presence of a PBG adduct on Cys1499 of the AWS Zn-finger (Fig. 3E). Accordingly, NBT and IAF staining confirmed that PBG could form quinoprotein adducts on AWS Zn-finger cysteines and induce Zn release (Supplemental Fig. 2, B–D). Interestingly, the 1499 cysteine residue chelates a Zn atom present in the AWS Zn-finger (Yang et al., 2016). However, as the peptide coverage was rather low (∼30%), we cannot rule out that other cysteines could be adducted. Further experiments carried out with the purified AWS Zn-finger domain confirmed that BQ could form covalent adducts with AWS Zn-finger cysteines and induce Zn release and protein crosslinks/oligomers (Supplemental Fig. 2, D and E). Consistent with our results, we found that *N,N,N',N'*-tetrakis-(2-pyridylmethyl)ethylenediamine (TPEN), a well known Zn chelator, could inactivate SETD2 catalytic domain by depleting Zn atoms (Supplemental Fig. 3). Altogether, our results suggest that BQ binds covalently to AWS domain Zn-finger cysteines within SETD2 catalytic domain, resulting in Zn release, loss of histone methyltransferase activity, and protein crosslinks/oligomers formation. This is in agreement with the key structural and functional role of the AWS Zn-finger domain of SETD2 (Yang et al., 2016; Zhang et al., 2017).

Impairment of SETD2 Histone Methyltransferase Activity and Decreased H3K36me3 Levels in Cells Exposed to BQ. We further tested the potential relevance of BQ-dependent inactivation of SETD2 by conducting

immunodetection of plumbagin adducts, plumbagin-treated SETD2 samples were separated by SDS-PAGE and transferred onto a nitrocellulose membrane. Plumbagin adducts were detected using an antibody against plumbagin. Ponceau staining of each nitrocellulose membrane is carried out to ensure equal protein loading. (D) Recombinant SETD2 was incubated with 30 μM PBG and 100 μM PAR for 20 minutes at room temperature. The absorbance of PAR-Zn^2 complexes (490 nm) was followed every minute using a plate reader. (E) Recombinant AWS domain was incubated with 30 μM PBG for 30 minutes at room temperature. The sample was then reduced with 10 mM DTT and alkylated with NEM prior to trypsin digestion and liquid chromatography–MS/MS analysis. The mass spectrum shows the presence of a plumbagin adduct on the Zn-finger cysteine residue 1499. The localization of the adduct on cysteine 1499 in AWS domain is displayed (inset).

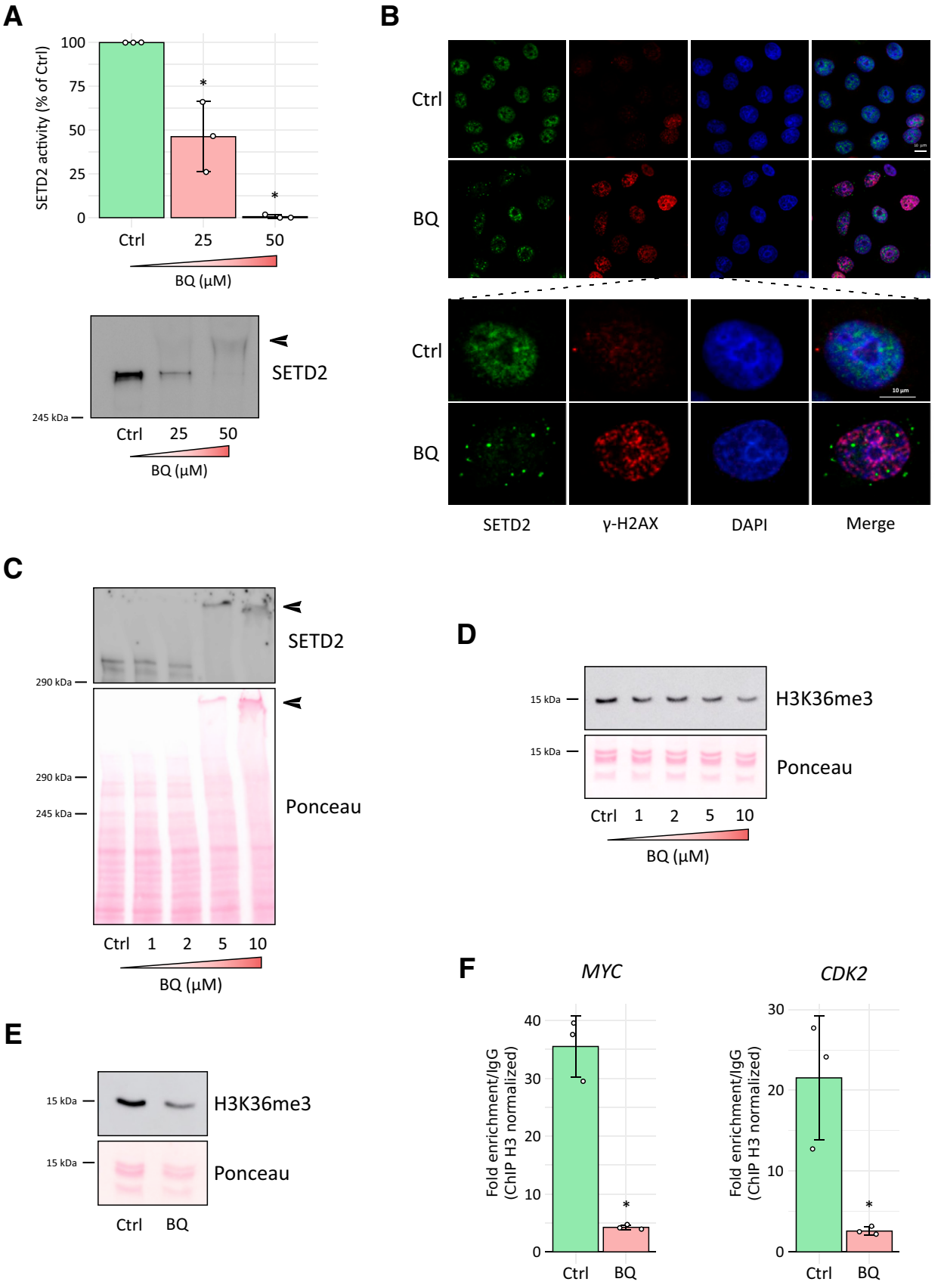

Fig. 4. BQ inhibits SETD2 activity and decreases H3K36me3 epigenetic mark in cells. (A) HEK293T cells transfected with full-length GFP-SETD2 plasmid were lysed, and 1 mg of cellular protein extracts was incubated with increasing concentrations of BQ (0–50 μM) for 30 minutes on ice. GFP-SETD2 was then immunoprecipitated, and residual SETD2 activity was measured by UFLC using a H3K36 fluorescent peptide. Bar

experiments in cells. To this end, the effects of BQ were first analyzed in HEK293T cells expressing GFP-tagged SETD2. This cellular approach has notably been used to analyze the formation of SETD2 aggregates/oligomers by Western blot (Bhattacharya and Workman, 2020). As shown in Fig. 4A, exposure of transfected cells to BQ led to the formation of inactive SETD2 crosslinks/oligomers as previously observed for other enzymes inhibited by BQ (Shu et al., 2020a, 2020b). SETD2 is inherently prone to protein crosslink/aggregation, and SETD2 aggregates/oligomers have been observed by immunofluorescence as puncta in cells (Bhattacharya and Workman, 2020). As shown in Fig. 4B, immunofluorescence studies showed the presence of puncta of SETD2 upon exposure of cells to BQ, thus supporting the formation of SETD2 crosslinks/oligomers as previously observed by Bhattacharya and Workman (2020). Further experiments were conducted in human hematopoietic K562 cells, which express functional SETD2. Consistent with the results described above, we found that exposure of K562 cells to BQ led to the formation of endogenous SETD2 crosslinks/oligomers (Fig. 4C). Concomitantly, and in agreement with the data reported above, we observed significantly decreased levels of the H3K36me3 mark on histones extracted from BQ-treated K562 cells (Fig. 4D). Congruent with the results obtained with the K562 cell line, exposure of human primary hematopoietic CD34+ stem cells to BQ led also to decrease of the H3K36me3 mark, which is consistent with inactivation of SETD2 by BQ (Fig. 4E). H3K36me3 levels have been shown to be present along the gene body with preference for exons, notably in *MYC* and *CDK2* genes (Eastmond et al., 2005). Using ChIP-qPCR, we analyzed the H3K36me3 levels at exons of *MYC* and *CDK2* in K562 cells exposed to BQ, as described previously by Hacker et al. (2016). Congruent with the above results, significantly decreased levels of H3K36me3 were observed for the exons studied, further supporting that BQ alters SETD2-dependent H3K36me3 epigenetic marks (Fig. 4F).

Discussion

BQ is considered as the major hematotoxic metabolite of BZ (Smith, 2010; North et al., 2020). The leukemogenic properties of BQ are thought to rely, at least in part, on the formation of covalent Michael adducts with cysteine residues that may affect the structure and the function of proteins involved in the regulation of hematopoietic cells (Smith et al., 2011; Bolton and Dunlap, 2017; North et al., 2020; Shu et al., 2020b). So far, inhibition of topoisomerase II enzymes by BQ is considered as one of the key mechanisms contributing to BZ hematotoxicity (Bender et al., 2007; Eastmond et al., 2014; Holmes and Winn, 2019). However, recent studies suggest that epigenetic mechanisms, notably DNA and histone methylation, could be altered in BZ-induced leukemogenesis (Yu et al., 2019; Chung and Herceg, 2020). We show here that the histone H3K36-specific trimethyltransferase SETD2 is inactivated by BQ. SETD2 is the sole lysine methyltransferase that catalyzes the formation of H3K36me3, a key epigenetic mark involved in transcriptional activation and DNA repair (Husmann and Gozani, 2019). SETD2 is considered as a tumor suppressor, and recurrent inactivating mutations of SETD2 and aberrant H3K36me3 levels have been reported in hematopoietic malignancies (Mar et al., 2014; Zhu et al., 2014; Husmann and Gozani, 2019). We found that BQ-dependent irreversible inactivation of SETD2 activity occurs through the formation of covalent BQ adducts on Zn-fingers cysteines present in the catalytic domain of the enzyme, notably within the AWS subdomain (Fig. 3; Supplemental Fig. 3). The formation of these quinoprotein adducts on SETD2 result in Zn release from the enzyme. It has been shown that Zn-bound cysteines in Zn-fingers are redox-sensitive and react readily with electrophilic compounds to form covalent adducts that are accompanied by Zn ejection and alteration of protein structure and function (Lee et al., 2013). Interestingly, the histone methyltransferases G9a and GLP are inhibited by electrophilic compounds able to eject Zn from Zn-fingers from their catalytic domain (Lenstra et al., 2018). Moreover, quinone-containing compounds have been reported to inhibit the histone demethylase KDM4A and the CREBBP/p300 acetyltransferase at least in part through Zn ejection from their catalytic Zn-finger domains (Jayatunga et al., 2015; Zhang et al., 2021). We also found that generation of BQ adducts on cysteine Zn-fingers within SETD2 catalytic domain led to the formation of protein crosslinks/oligomers that may contribute to enzyme inactivation (Figs. 2 and 4). This is consistent with observations indicating that disruption of Zn-bound cysteines in Zn-fingers, notably through oxidation or reaction with electrophiles, can lead to Zn release and subsequent protein unfolding (Quintal et al., 2011; Lee et al., 2013; Kluska et al., 2018). Interestingly, SETD2 has been shown to be a rather unstable protein and prone to aggregation (Bhattacharya and Workman, 2020).

plots and error bars represent the means and the S.D. of three independent experiments, respectively. *$P < 0.05$ compared with Ctrl. In parallel, half of the immunoprecipitated samples was separated by SDS-PAGE and transferred onto a nitrocellulose membrane. GFP-SETD2 protein was detected using an anti-GFP antibody against GFP. Black arrows represent high-molecular-weight SETD2 protein crosslinks/oligomers. (B) HeLa cells were exposed to 20 μM BQ for 30 minutes at 37°C, washed, and further cultured for 6 hours at 37°C in fresh medium. Cells were fixed with methanol for 15 minutes, and endogenous SETD2 was detected by immunofluorescence using a specific anti-SETD2 antibody. An antibody against γ-H2AX protein was also used to evaluate BQ-dependent DNA breaks. DAPI staining is featured for nuclear localization. Optical sections are shown with scale bars of 10 μm. (C) K562 cells were exposed to increasing concentrations of BQ (0–10 μM) for 30 minutes at 37°C and then washed and further cultured for 3 hours at 37°C in fresh medium. Cells were then lysed, and protein extracts were separated by SDS-PAGE and transferred onto a nitrocellulose membrane. Endogenous SETD2 protein was detected using an anti-SETD2 antibody. Ponceau staining is shown. Black arrows represent high-molecular-weight SETD2 protein crosslinks/oligomers. (D) Endogenous histones were extracted from K562 cell lysates, and 2.5 μg of extracted histones was separated by SDS-PAGE and transferred onto a nitrocellulose membrane. Levels of the H3K36me3 mark were detected using an anti-H3K36me3 antibody. Ponceau staining was carried out to ensure equal protein loading. (E) Human hematopoietic $CD34^+$ cells were exposed to 10 μM BQ for 30 minutes at 37°C, washed, and further incubated for 3 hours in fresh medium. Cells were then lysed into Laemmli Buffer containing 400 mM β-mercaptoethanol. Samples were separated by SDS-PAGE and transferred onto a nitrocellulose membrane. Levels of the H3K36me3 mark were detected using an anti-H3K36me3 antibody. Ponceau staining was carried out to ensure equal protein loading. (F) K562 cells were exposed to 10 μM BQ for 30 minutes at 37°C, washed, and further cultured for 3 hours at 37°C in fresh medium. ChIP was carried out using antibodies against H3K36me3 histone mark and H3 as described in *Materials and Methods*. RT-qPCR experiments were subsequently carried out on human *MYC* and *CDK2* genes using primers specific for exons 3 and 6, respectively, located in the gene bodies.

More broadly, protein crosslinking upon covalent binding of BQ to cysteines has been shown to occur with enzymes such as glyceraldehyde-3-phosphate dehydrogenase, creatine kinase or thioredoxin 1, and is thought to be responsible, at least in part, for their inhibition (Shu et al., 2020a, 2020b). Moreover, the findings obtained with the purified SETD2 catalytic domain were further supported by experiments carried out in cells. Indeed, we found that exposure to BQ of cells expressing ectopically GFP-SETD2 or endogenous SETD2 resulted in protein crosslinks/oligomers and loss of SETD2 activity as observed with the purified SETD2 catalytic domain (Figs. 2 and 4). Consistent with this, we found that exposure to BQ caused a marked decrease of the H3K36me3 mark on histones from human hematopoietic K562 or primary bone marrow CD34+ cells. SETD2 activity and trimethylation of H3K36 are involved in normal hematopoiesis, and alteration of SETD2 and H3K36me3 levels is recurrently observed in hematopoietic malignancies (Mar et al., 2017; Chen et al., 2020). Of note, dysregulation of epigenetic processes such as DNA and histone methylation by BZ has been reported over the last years (Smith, 2010; Fenga et al., 2016; Chung and Herceg, 2020). Our data support these observations and provide mechanistic evidence that BQ, an oxidative and hematotoxic metabolite of BZ, is able to react with and perturb the activity of a key epigenetic enzyme.

Acknowledgments

We thank the technical platform "BioProfiler" (BFA, CNRS UMR 8251 Unit, Université de Paris) for provision of UFLC facilities.

Authorship Contributions

Participated in research design: Berthelet, Guidez, Rodrigues-Lima.

Conducted experiments: Berthelet, Michail, Bui, Le Coadou, Sirri, Guidez.

Performed data analysis: Berthelet, Michail, Bui, Le Coadou, Sirri, Wang, Dulphy, Dupret, Chomienne, Guidez, Rodrigues-Lima.

Wrote or contributed to the writing of the manuscript: Berthelet, Rodrigues-Lima.

References

Bender RP, Ham A-JJL, and Osheroff N (2007) Quinone-induced enhancement of DNA cleavage by human topoisomerase IIalpha: adduction of cysteine residues 392 and 405. *Biochemistry* **46**:2856–2864.

Bhattacharya S and Workman JL (2020) Regulation of SETD2 stability is important for the fidelity of H3K36me3 deposition. *Epigenetics Chromatin* **13**:40.

Bolton JL and Dunlap T (2017) Formation and biological targets of quinones: Cytotoxic versus cytoprotective effects. *Chem Res Toxicol* **30**:13–37.

Butler JS and Dent SYR (2013) The role of chromatin modifiers in normal and malignant hematopoiesis. *Blood* **121**:3076–3084.

Chappell G, Pogribny IP, Guyton KZ, and Rusyn I (2016) Epigenetic alterations induced by genotoxic occupational and environmental human chemical carcinogens: a systematic literature review. *Mutat Res Rev Mutat Res* **768**:27–45.

Chen BY, Song J, Hu CL, Chen SB, Zhang Q, Xu CH, Wu JC, Hou D, Sun M, Zhang YL, et al. (2020) SETD2 deficiency accelerates MDS-associated leukemogenesis via S100a9 in NHD13 mice and predicts poor prognosis in MDS. *Blood* **135**:2271–2285.

Chopra M and Bohlander SK (2015) Disturbing the histone code in leukemia: translocations and mutations affecting histone methyl transferases. *Cancer Genet* **208**:192–205.

Chung FFL and Herceg Z (2020) The promises and challenges of toxico-epigenomics: Environmental chemicals and their impacts on the epigenome. *Environ Health Perspect* **128**:15001.

Copeland RA (2005) Evaluation of enzyme inhibitors in drug discovery. A guide for medicinal chemists and pharmacologists. *Methods Biochem Anal* **46**:1–265.

Dong Y, Zhao X, Feng X, Zhou Y, Yan X, Zhang Y, Bu J, Zhan D, Hayashi Y, Zhang Y, et al. (2019) SETD2 mutations confer chemoresistance in acute myeloid leukemia partly through altered cell cycle checkpoints. *Leukemia* **33**:2585–2598.

Duval R, Bui LC, Mathieu C, Nian Q, Berthelet J, Xu X, Haddad I, Vinh J, Dupret JM, Busi F, et al. (2019) Benzoquinone, a leukemogenic metabolite of benzene, catalytically inhibits the protein tyrosine phosphatase PTPN2 and alters STAT1 signaling. *J Biol Chem* **294**:12483–12494.

Duval R, Fritsch L, Bui L-C, Berthelet J, Guidez F, Mathieu C, Dupret J-M, Chomienne C, Ait-Si-Ali S, and Rodrigues-Lima F (2015) An acetyltransferase assay for CREB-binding protein based on reverse phase-ultra-fast liquid chromatography of fluorescent histone H3 peptides. *Anal Biochem* **486**:35–37.

Eastmond DA, Keshava N, and Sonawane B (2014) Lymphohematopoietic cancers induced by chemicals and other agents and their implications for risk evaluation: An overview. *Mutat Res* **761**:40–64.

Eastmond DA, Mondrala ST, and Hasegawa L (2005) Topoisomerase II inhibition by myeloperoxidase-activated hydroquinone: a potential mechanism underlying the genotoxic and carcinogenic effects of benzene. *Chem Biol Interact* **153-154**:207–216.

Edmunds JW, Mahadevan LC, and Clayton AL (2008) Dynamic histone H3 methylation during gene induction: HYPB/Setd2 mediates all H3K36 trimethylation. *EMBO J* **27**:406–420.

Fahey CC and Davis IJ (2017) SETting the stage for cancer development: SETD2 and the consequences of lost methylation. *Cold Spring Harb Perspect Med* **7**:a026468.

Fenga C, Gangemi S, and Costa C (2016) Benzene exposure is associated with epigenetic changes (review). Review *Mol Med Rep* **13**:3401–3405.

Frantz CE, Chen H, and Eastmond DA (1996) Inhibition of human topoisomerase II in vitro by bioactive benzene metabolites. *Environ Health Perspect* **104** (Suppl 6):1319–1323.

Hacker KE, Fahey CC, Shinsky SA, Chiang YJ, DiFiore JV, Jha DK, Vo AH, Shavit JA, Davis IJ, Strahl BD, et al. (2016) Structure/function analysis of recurrent mutations in SETD2 protein reveals a critical and conserved role for a SET domain residue in maintaining protein stability and histone H3 Lys-36 trimethylation. *J Biol Chem* **291**:21283–21295.

Holmes TH and Winn LM (2019) DNA damage and perturbed topoisomerase IIα as a target of 1,4-benzoquinone toxicity in murine fetal liver cells. *Toxicol Sci* **171**:339–346.

Huether R, Dong L, Chen X, Wu G, Parker M, Wei L, Ma J, Edmonson MN, Hedlund EK, Rusch MC, et al. (2014) The landscape of somatic mutations in epigenetic regulators across 1,000 paediatric cancer genomes. *Nat Commun* **5**:3630.

Husmann D and Gozani O (2019) Histone lysine methyltransferases in biology and disease. *Nat Struct Mol Biol* **26**:880–889.

Jayatunga MKP, Thompson S, McKee TC, Chan MC, Reece KM, Hardy AP, Sekirnik R, Seden PT, Cook KM, McMahon JB, et al. (2015) Inhibition of the HIF1α-p300 interaction by quinone- and indandione-mediated ejection of structural Zn(II). *Eur J Med Chem* **94**:509–516.

Kim S, Vermeulen R, Waidyanatha S, Johnson BA, Lan Q, Rothman N, Smith MT, Zhang L, Li G, Shen M, et al. (2006a) Using urinary biomarkers to elucidate dose-related patterns of human benzene metabolism. *Carcinogenesis* **27**:772–781.

Kim S, Vermeulen R, Waidyanatha S, Johnson BA, Lan Q, Smith MT, Zhang L, Li G, Shen M, Yin S, et al. (2006b) Modeling human metabolism of benzene following occupational and environmental exposures. *Cancer Epidemiol Biomarkers Prev* **15**:2246–2252.

Kluska K, Adamczyk J, and Krężel A (2018) Metal binding properties, stability and reactivity of zinc fingers. *Coord Chem Rev* **367**:18–64.

Kudithipudi S and Jeltsch A (2014) Role of somatic cancer mutations in human protein lysine methyltransferases. *Biochim Biophys Acta* **1846**:366–379.

Lee YM, Wang YT, Duh Y, Yuan HS, and Lim C (2013) Identification of labile Zn sites in drug-target proteins. *J Am Chem Soc* **135**:14028–14031.

Lenstra DC, Al Temimi AHK, and Mecinović J (2018) Inhibition of histone lysine methyltransferases G9a and GLP by ejection of structural Zn(II). *Bioorg Med Chem Lett* **28**:1234–1238.

Li J, Duns G, Westers H, Sijmons R, van den Berg A, and Kok K (2016) SETD2: an epigenetic modifier with tumor suppressor functionality. *Oncotarget* **7**:50719–50734.

Lu PCW, Shahbaz S, and Winn LM (2020) Benzene and its effects on cell signaling pathways related to hematopoiesis and leukemia. *J Appl Toxicol* **40**:1018–1032.

Mar BG, Bullinger LB, McLean KM, Grauman PV, Harris MH, Stevenson K, Neuberg DS, Sinha AU, Sallan SE, Silverman LB, et al. (2014) Mutations in epigenetic regulators including SETD2 are gained during relapse in paediatric acute lymphoblastic leukaemia. *Nat Commun* **5**:3469.

Mar BG, Chu SH, Kahn JD, Krivtsov AV, Koche R, Castellano CA, Kotlier JL, Zon RL, McConkey ME, Chabon J, et al. (2017) *SETD2* alterations impair DNA damage recognition and lead to resistance to chemotherapy in leukemia. *Blood* **130**:2631–2641.

Mbiya W, Chipinda I, Siegel PD, Mhike M, and Simoyi RH (2013) Substituent effects on the reactivity of benzoquinone derivatives with thiols. *Chem Res Toxicol* **26**:112–123.

McHale CM, Zhang L, and Smith MT (2012) Current understanding of the mechanism of benzene-induced leukemia in humans: implications for risk assessment. *Carcinogenesis* **33**:240–252.

North CM, Rooseboom M, Kocabas NA, Schnatter AR, Faulhammer F, and Williams SD (2020) Modes of action considerations in threshold expectations for health effects of benzene. *Toxicol Lett* **334**:78–86.

Quintal SM, dePaula QA, and Farrell NP (2011) Zinc finger proteins as templates for metal ion exchange and ligand reactivity. Chemical and biological consequences. *Metallomics* **3**:121–139.

Lindsey RH Jr, Bromberg KD, Felix CA, and Osheroff N (2004) 1,4-Benzoquinone is a topoisomerase II poison. *Biochemistry* **43**:7563–7574.

Rappaport SM, Kim S, Lan Q, Li G, Vermeulen R, Waidyanatha S, Zhang L, Yin S, Smith MT, and Rothman N (2010) Human benzene metabolism following occupational and environmental exposures. *Chem Biol Interact* **184**:189–195.

Sauer E, Gauer B, Nascimento S, Nardi J, Göethel G, Costa B, Correia D, Matte U, Charão M, Arbo M, et al. (2018) The role of B7 costimulation in benzene immunotoxicity and its potential association with cancer risk. *Environ Res* **166**:91–99.

Shu N, Cheng Q, Arnér ESJ, and Davies MJ (2020a) Inhibition and crosslinking of the selenoprotein thioredoxin reductase-1 by p-benzoquinone. *Redox Biol* **28**:101335.

Shu N, Hägglund P, Cai H, Hawkins CL, and Davies MJ (2020b) Modification of Cys residues in human thioredoxin-1 by p-benzoquinone causes inhibition of its catalytic activity and activation of the ASK1/p38-MAPK signalling pathway. *Redox Biol* **29**:101400.

Shu N, Lorentzen LG, and Davies MJ (2019) Kinetics and biological consequences of quinone-induced protein adduction. *Free Radic Biol Med* **120**:S55.
Smith MT (2010) Advances in understanding benzene health effects and susceptibility. *Annu Rev Public Health* **31**:133–148, 2, 148.
Smith MT, Zhang L, McHale CM, Skibola CF, and Rappaport SM (2011) Benzene, the exposome and future investigations of leukemia etiology. *Chem Biol Interact* **192**:155–159.
Snyder R (2012) Leukemia and benzene. *Int J Environ Res Public Health* **9**:2875–2893.
Wagner EJ and Carpenter PB (2012) Understanding the language of Lys36 methylation at histone H3. *Nat Rev Mol Cell Biol* **13**:115–126.
Wang L, Niu N, Li L, Shao R, Ouyang H, and Zou W (2018) H3K36 trimethylation mediated by SETD2 regulates the fate of bone marrow mesenchymal stem cells. *PLoS Biol* **16**:e2006522.
Wang X, Thomas B, Sachdeva R, Arterburn L, Frye L, Hatcher PG, Cornwell DG, and Ma J (2006) Mechanism of arylating quinone toxicity involving Michael adduct formation and induction of endoplasmic reticulum stress. *Proc Natl Acad Sci USA* **103**:3604–3609.
Whysner J, Reddy MV, Ross PM, Mohan M, and Lax EA (2004) Genotoxicity of benzene and its metabolites. *Mutat Res* **566**:99–130.
Yang S, Zheng X, Lu C, Li G-MM, Allis CD, and Li H (2016) Molecular basis for oncohistone H3 recognition by SETD2 methyltransferase. *Genes Dev* **30**: 1611–1616.
Yu C-HH, Li Y, Zhao X, Yang S-QQ, Li L, Cui N-XX, Rong L, and Yi Z-CC (2019) Benzene metabolite 1,2,4-benzenetriol changes DNA methylation and histone acetylation of erythroid-specific genes in K562 cells. *Arch Toxicol* **93**: 137–147.
Zhang W, Berthelet J, Michail C, Bui LC, Gou P, Liu R, Duval R, Renault J, Dupret JM, Guidez F, et al. (2021) Human CREBBP acetyltransferase is impaired by etoposide quinone, an oxidative and leukemogenic metabolite of the anticancer drug etoposide through modification of redox-sensitive zinc-finger cysteine residues. *Free Radic Biol Med* **162**:27–37.
Zhang Y-LL, Sun J-WW, Xie Y-YY, Zhou Y, Liu P, Song J-CC, Xu C-HH, Wang L, Liu D, Xu A-NN, et al. (2018) Setd2 deficiency impairs hematopoietic stem cell self-renewal and causes malignant transformation. *Cell Res* **28**:476–490.
Zhang Y, Shan C-MM, Wang J, Bao K, Tong L, and Jia S (2017) Molecular basis for the role of oncogenic histone mutations in modulating H3K36 methylation. *Sci Rep* **7**:43906.
Zhou Y, Yan X, Feng X, Bu J, Dong Y, Lin P, Hayashi Y, Huang R, Olsson A, Andreassen PR, et al. (2018) *Setd2* regulates quiescence and differentiation of adult hematopoietic stem cells by restricting RNA polymerase II elongation. *Haematologica* **103**:1110–1123.
Zhu X, He F, Zeng H, Ling S, Chen A, Wang Y, Yan X, Wei W, Pang Y, Cheng H, et al. (2014) Identification of functional cooperative mutations of SETD2 in human acute leukemia. *Nat Genet* **46**:287–293.

Address correspondence to: Fernando Rodrigues-Lima, Université de Paris, BFA, UMR 8251, CNRS, F-75013, Paris, France. E-mail: fernando.rodrigues-lima@univ-paris-diderot

SUPPLEMENTAL FIGURES

The benzene hematotoxic and reactive metabolite 1,4-benzoquinone impairs the activity of the histone methyltransferase SETD2 and causes aberrant H3K36 trimethylation (H3K36me3)

Jérémy Berthelet[1,#], Christina Michail[1], Linh-Chi Bui[1], Louise Le Coadou[1], Valentina Sirri[1], Li Wang[2], Nicolas Dulphy[3], Jean-Marie Dupret[1], Christine Chomienne[4,5], Fabien Guidez[4] and Fernando Rodrigues-Lima[1]

[1] Université de Paris, Unité de Biologie Fonctionnelle et Adaptative (BFA), UMR 8251, CNRS, 75013 Paris, France
[2] The First Affiliated Hospital of Chongqing Medical University, Department of Hematology, Chongqing, China
[3] Université de Paris, Institut de Recherche Saint-Louis (IRSL), UMRS 1160, INSERM, 75010 Paris, France
[4] Université de Paris, Institut de Recherche Saint-Louis (IRSL), UMRS 1131, INSERM, 75010 Paris, France
[5] Service de Biologie Cellulaire, Assistance Publique des Hôpitaux de Paris (AP-HP), Hôpital Saint Louis, Paris, France

[#] Present address: Université de Paris, Centre Epigénétique et Destin Cellulaire (CEDC), UMR 7216, CNRS, 75013, Paris, France.

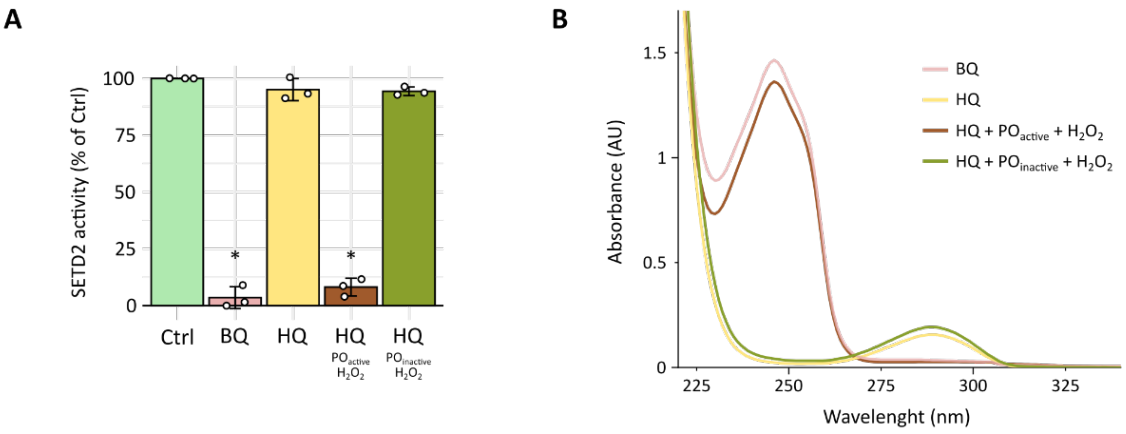

Sup figure 1. (A) Recombinant SETD2 was incubated 30 µM BQ or HQ or HQ preincubated with active (HQ PO active) or inactive peroxidase (HQ inactive PO) hydroquinone-bioactivation system (see Materials and Methods) for 10 min at room temperature. Residual SETD2 activity was measured by UFLC using a H3K36 fluorescent peptide. Barplots and error bars represent the means and the SD of three independent experiments, respectively. * : *p.value* < 0.05 compared with control (Ctrl). **(B)** Absorbance spectrum (220-340 nm) of BQ, or HQ or HQ in the presence of active (HQ PO active) or inactive peroxidase (HQ PO inactive) bioactivation system (see Materials and Methods). Co-incubation of HQ with active PO hydroquinone-bioactivation system leads to a shift in the HQ absorbance spectrum with the loss of the characteristic HQ peak at 290 nm and the apparition of the characteristic BQ peak at 245 nm.

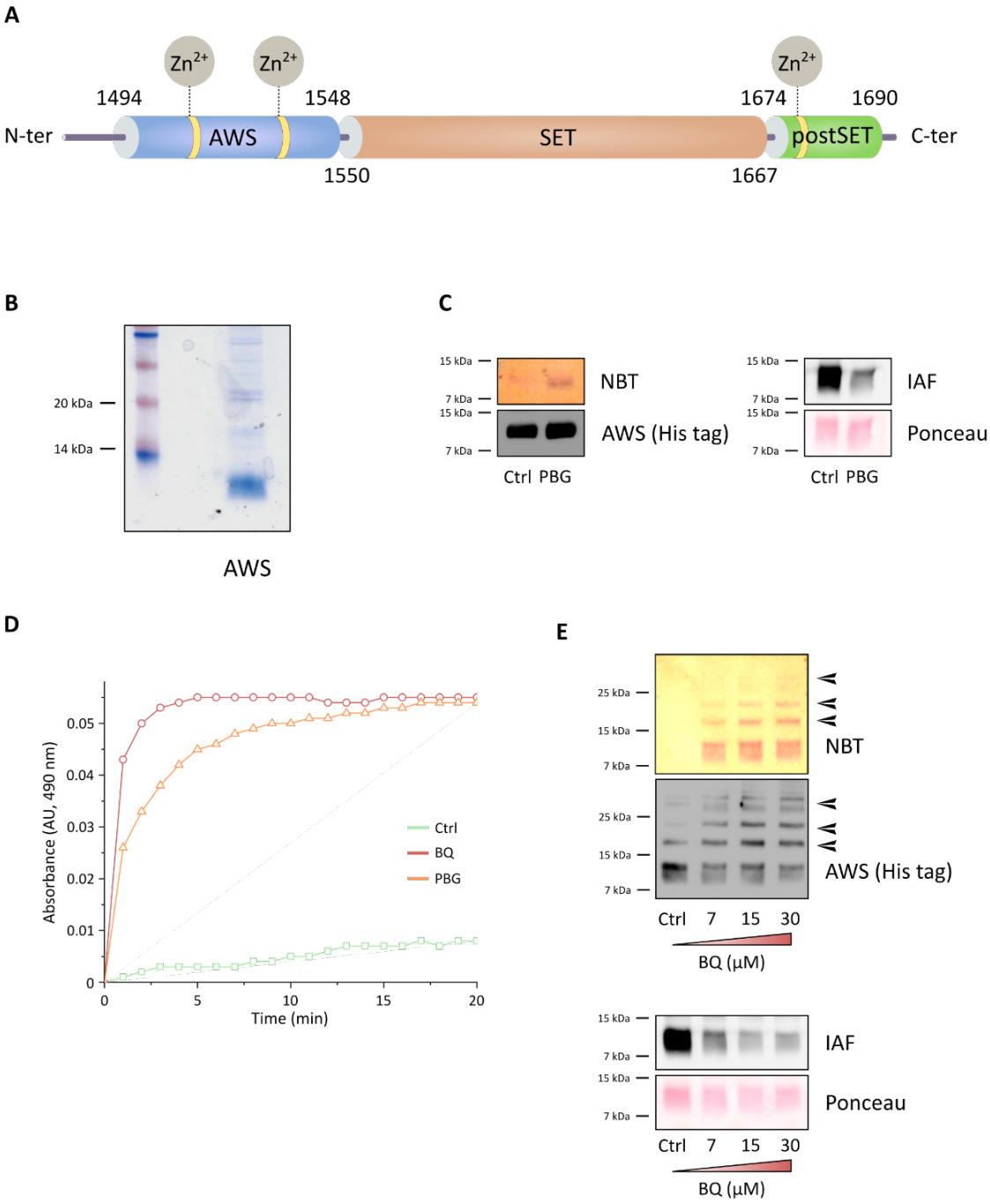

Sup figure 2. (A) Schematic representation of the catalytic domain of SETD2. Locations of the zinc fingers are represented using grey spheres. The AWS domain is displayed in blue, SET domain in light brown and post-SET domain in green. **(B)** Recombinant AWS domain of SETD2 was separated by SDS-PAGE followed by Coomassie staining. **(C)** Recombinant AWS domain of SETD2 was incubated with 30 µM plumbagin (PBG) for 15 min at room temperature. Left panel: For the nitro blue tetrazolium (NBT) staining of quinoprotein adducts, samples were separated by SDS-PAGE and transferred onto a nitrocellulose membrane. Plumbagin adducts on the AWS domain were then detected using NBT staining as described in Materials and Methods. Right panel: For the iodoacetamide-fluorescein (IAF) cysteine labelling, samples were incubated with 20 µM iodoacetamide-fluorescein (IAF) for 10 min at 37°C. Samples were then separated by SDS-PAGE and transferred onto a nitrocellulose membrane. IAF-labelled cysteine residues were detected by fluorescence emission (λ_{exc}= 485 nm, λ_{em}= 530 nm). Ponceau staining is shown. **(D)** Recombinant AWS domain of SETD2 (5 µg) was incubated in the presence of 30 µM

1,4-benzoquinone (BQ) or plumbagin (PBG) and 100 µM 4-(2-pyridylazo)resorcinol (PAR) for 20 min at room temperature. The absorbance of PAR-Zn^2-complexes (490 nm) was followed every minute using a plate reader. **(E)** Recombinant AWS domain of SETD2 was incubated with increasing concentrations of BQ (0-30 µM) for 10 min at room temperature. Top panel: For the nitro blue tetrazolium (NBT) staining of quinoprotein adducts, samples were separated by SDS-PAGE and transferred onto a nitrocellulose membrane. BQ adducts on the AWS domain were then detected using NBT staining as described in Materials and Methods. The same samples were also analyzed by Western blot using an anti-6xHistidine tag antibody. Black arrows represent high molecular weight SETD2 protein cross-links/oligomers. Bottom panel: For the iodoacetamide-fluorescein (IAF) cysteine labelling, samples were incubated with 20 µM iodoacetamide-fluorescein (IAF) for 10 min at 37°C, separated by SDS-PAGE and transferred onto a nitrocellulose membrane. IAF-labelled cysteine residues were detected by fluorescence emission (λ_{exc}= 485 nm, λ_{em}= 530 nm). Ponceau staining is shown.

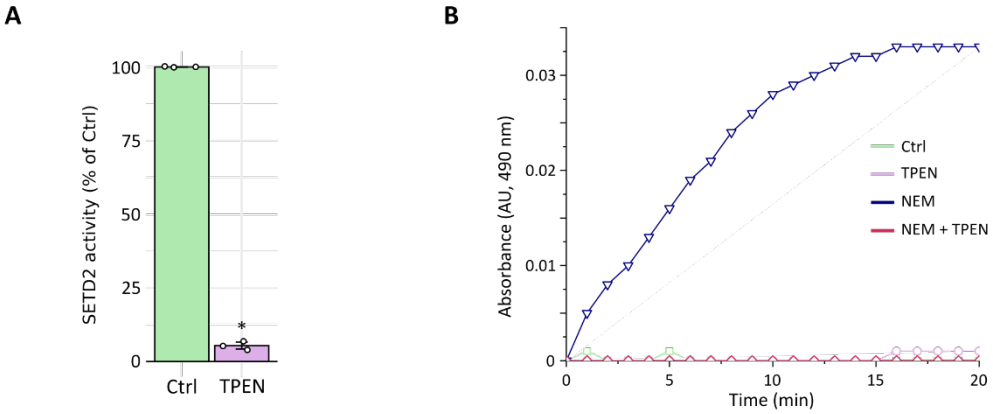

Sup figure 3. (A) Recombinant SETD2 (3 µM) was incubated with 1 mM *N*,*N*,*N'*,*N'*-tetrakis(2-pyridinylmethyl)-1,2-ethanediamine (TPEN) for 10 min at room temperature, followed by a buffer exchange using PD-10 columns to methyltransferase buffer (see Materials and Methods). Residual SETD2 activity was measured by UFLC using H3K36 fluorescent peptide. Barplots and error bars represent the means and the SD of three independent experiments, respectively. * : *p.value* < 0.05 compared with control (Ctrl). **(B)** Recombinant SETD2 (3 µM) was incubated in the presence of 1 mM TPEN for 10 min at room temperature, followed by a buffer exchange using PD-10 columns to SETD2 activity buffer (see Materials and Methods). SETD2 (1 µM) was then incubated with 1 mM *N*-ethylmaleimide (NEM) and 100 µM 4-(2-pyridylazo)resorcinol (PAR) for 20 min at room temperature. The absorbance of PAR-Zn^2-complexes (490 nm) was followed every minute using a plate reader.